



Comparisons of the Microstructure and Magnetic Properties of Anisotropic NdFeB Magnets Prepared by Hot Pressing and Spark Plasma Sintering

Xiang Li¹ · Qing-Zheng Jiang^{1,2} · Sajjad Ur Rehman¹ · Qing-Fang Huang^{1,2} · You-Wei Chen¹ · Chuan-Jia Zhao¹ · Zhen-Chen Zhong¹

Received: 29 September 2021 / Accepted: 7 October 2021 / Published online: 19 October 2021
© The Author(s), under exclusive licence to Springer Science+Business Media, LLC, part of Springer Nature 2021

Abstract

NdFeB hot-pressed and hot-deformed magnets were prepared by hot-pressed (HP) sintering and spark plasma sintering (SPS). The effects of sintering mechanisms of SPS and HP on the microstructure of hot deformation magnets were studied. The temperature of the mold surface is much higher than that of the sample in the cavity in HP, but lower than that of the sample in SPS. The Nd-rich phase is uniformly distributed and the grain size is smaller in the hot-deformed magnets prepared by HP, while the Nd-rich phase is excessively enriched and the grain size in the liquid-enriched region is abnormal in the hot-deformed magnets prepared by SPS. The comprehensive magnetic properties of hot deformed magnets prepared by SPS are significantly lower than those prepared by HP.

Keywords NdFeB magnets · Hot pressing · Spark plasma sintering · Microstructure · Magnetic properties

1 Introduction

Since the hot-deformed NdFeB magnets discovered by Lee et al. [1] in 1984, nanocrystalline permanent magnets have attracted great interest [2–6]. Because of their good magnetic properties, excellent thermal stability, and better corrosion resistance, these alloys have great value in practical application. However, it is well known that when the grains in the magnets are overgrown, the microstructure tends to change from small flat platelet-shaped grains to large spherical grains and the grain alignment is disrupted [7, 8]. Moreover, when the Nd-rich phase gathers at the triple junction, the Nd concentration in the intergranular phase reduces, which is harmful to the magnetic isolation of the hard magnetic

grains [9]. Thus, it is necessary to determine the technology for preparing uniform microstructure magnets.

Hot-pressing (HP) and spark plasma sintering (SPS) are two effective techniques for preparing anisotropic magnets. In recent years, both HP and SPS have been applied to prepare hot-pressed magnets which can be subsequently subjected to hot deformation to prepare anisotropic magnets [10, 11]. Numerous studies on the microstructure and magnetic properties of hot-pressed and hot-deformed magnets sintered by HP or SPS have been carried out [12–16]. A comparison of the research findings reveals that the hot-pressed and hot-deformed magnets processed by SPS depict finer grain size and better properties because of the short processing time of SPS [17–22]. However, the above results were obtained from experimental data. Different raw materials, pressure, cylindrical dies, and measuring methods were used, which likely resulted in inaccurate comparison. In order to compare more accurately, the differences of microstructure, grain growth mode, and magnetic properties in different fabrication processes, the same raw materials, and measurement methods must be used for magnets prepared by HP and SPS. In other fields such as ceramics and oxides, direct comparative studies on the differences between HP and SPS have been systematically reported [23–25]. However, for hot-pressed/

✉ Qing-Zheng Jiang
jqz666@126.com

Zhen-Chen Zhong
zczhong2013@163.com

¹ Jiangxi Key Laboratory for Rare Earth Magnetic Materials and Devices & College of Rare Earths, Jiangxi University of Science and Technology, Ganzhou 341000, People's Republic of China

² Fujian Key Laboratory for Rare Earth Functional Materials, Longyan 366300, People's Republic of China

hot-deformed magnets, few studies systematically compare the differences between HP and SPS directly.

In this study, we have systematically studied the influence of HP and SPS on the microstructure, grain growth rate, and magnetic properties of the hot-deformed magnet. Interestingly, by scanning electron microscopy (SEM) analysis, it was found that the grain size of the sample prepared by SPS was larger than that of the sample prepared by HP, and the liquid phase was excessively enriched at triple junctions although the deformation temperature of HP is much higher than that of the SPS. This is contrary to the assumption that the use of SPS restrains the grain growth due to its low sintering temperature. The magnetic properties of the samples prepared by SPS are exceedingly deteriorated due to the large enrichment of liquid phase and the abnormal growth of grains [7, 9].

2 Material and Methods

2.1 Raw Materials

The magnetic powder of $\text{Nd}_{29.8}\text{Pr}_{0.1}\text{Fe}_{64.7}\text{Si}_{0.1}\text{Co}_{3.0}\text{Al}_{0.1}\text{Ga}_{0.5}\text{B}_{\text{bal}}$ (wt.%) was used as the raw material.

2.2 HP and SPS Experiments

For both the HP and SPS experiments, equal amounts of magnetic powders (10 g) were placed in a cylindrical alloy mold. The interior of the die and the surfaces of punches were covered with 0.2-mm-thick graphite foil. All the experiments were conducted in vacuum.

In hot-pressing, the sintering temperature and holding time were 650 °C and 5 min. The hot-pressed magnet prepared by HP is denoted as H_0 hereafter. With H_0 as the precursor, the HP was used to prepare the hot-deformed magnet. The hot deformation temperatures of the magnet were 780 °C, 800 °C, 820 °C, 840 °C, and 860 °C, with holding

time of 5 min. The hot-deformed magnets are respectively denoted as H780 °C, H800 °C, H820 °C, H840 °C, and H860 °C. (The initial deformation temperature of 780 °C is chosen because when the deformation temperature is lower than 780 °C, the magnet is not sufficiently softened and crushed during the deformation process due to the low temperature in the cavity.)

Independently, experiments were completed on the SPS furnace. The sintering conditions of SPS magnet are the same as those of H_0 . The magnet prepared by SPS is denoted by S_0 . With S_0 as the precursor, the hot deformation is undertaken at 600 °C, 650 °C, 700 °C, 750 °C, and 800 °C, with holding of 5 min. Five deformed magnets are respectively denoted as S600 °C, S650 °C, S700 °C, S750 °C, and S800 °C.

2.3 Characterization

The magnetic properties of hot-pressed magnets were measured with a hysteresis loop tracer, NIM500C. The density for the magnets was measured by the Archimedes principle. Small cylindrical magnets with a size of ϕ 2.6 mm, from the center of the hot-deformed magnet, were obtained for magnetic measurements. Then, magnetic properties of a small cylindrical magnet were obtained in physical property measurement system (PPMS) equipped with a 9.0-T vibrating sample magnetometer (VSM). X-ray diffraction patterns were obtained with X-ray diffractometer using $\text{Cu-K}\alpha$ radiation. The microstructure and chemical compositions were analyzed by scanning electron microscopy (SEM) and energy dispersion spectroscopy (EDS).

3 Results and Discussion

The demagnetization curves of H_0 and S_0 are depicted in Fig. 1(a). The squareness of demagnetization curves is denoted by the ratio H_k/H_{c2} , where H_k is defined as the demagnetizing field where the magnetization J reduces to

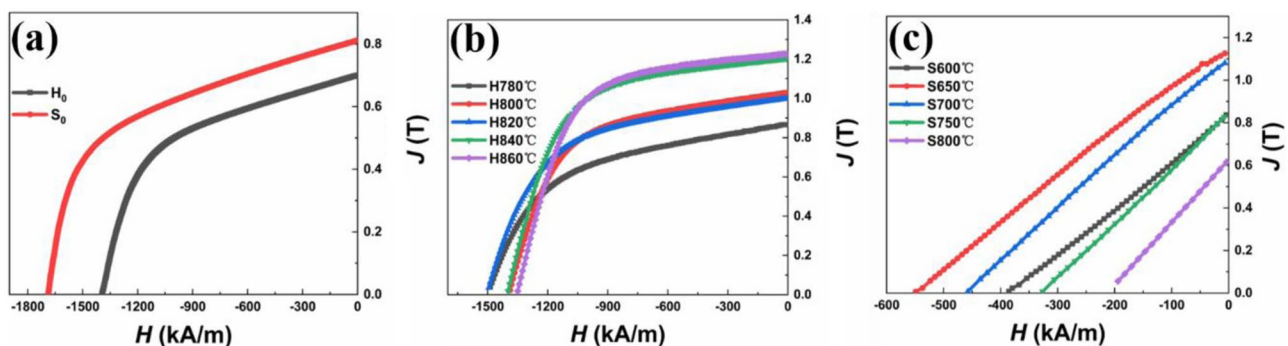


Fig. 1 (a) Demagnetization curves of hot-pressed magnet H_0 and S_0 prepared by HP and SPS respectively. (b) and (c) are demagnetization curves of hot-deformed magnets prepared by HP and SPS at different deformation temperatures

Table 1 Magnetic properties of H_0 and S_0

Sample	J_r (T)	H_{cj} (kA/m)	$(BH)_{max}$ (kJ/m ³)	Q
H_0	0.70	1395	86	0.55
S_0	0.81	1688	116	0.51

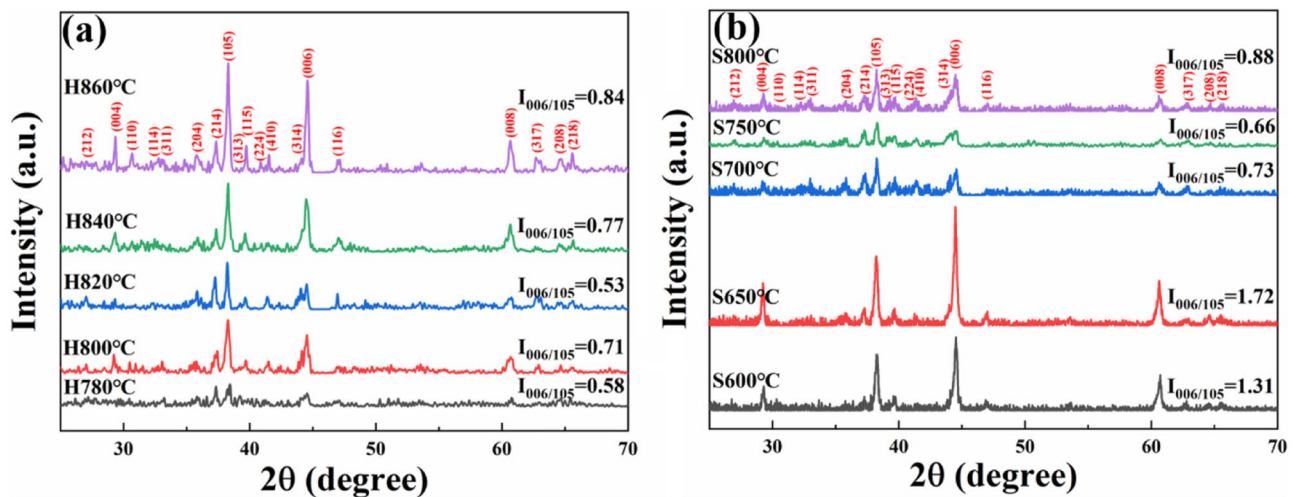
80% of J_r , whose value is obtained from the bottom of the small step in the initial demagnetization curve [26]. The squareness of samples H_0 is slightly higher than that of S_0 and its values are 0.55 and 0.51, respectively. The corresponding magnetic properties are listed in Table 1. Under the same sintering process, the magnetic property of H_0 prepared by HP is lower than that of S_0 prepared by SPS, which may be caused by the lower density of H_0 magnet [27].

Figure 1(b) shows the demagnetization curves of the hot-deformed magnets prepared by HP at different temperatures. The magnetic properties of H780 °C magnet are $H_{cj} = 1498$ kA/m, $J_r = 0.87$ T, and $(BH)_{max} = 132$ kJ/m³. The magnetic properties change with the increase of deformation temperature. When the temperature reaches 860 °C, the H_{cj} decreases and reaches 1354 kA/m, while the J_r increases to 1.23 T resulting in an enhanced $(BH)_{max} = 276$ kJ/m³. Figure 1(c) shows the demagnetization curves of the hot-deformed magnets prepared by SPS at different temperatures. Magnetic properties with increasing temperature show an increasing trend in the beginning, then decrease, and the best magnetic properties are obtained at 650 °C. The magnetic properties $H_{cj} = 551$ kA/m, $J_r = 1.12$ T, and $(BH)_{max} = 103$ kJ/m³ are obtained for S650 °C. There is a great difference between the magnetic properties of H860 °C and S650 °C magnet. The intrinsic coercivity of H860 °C is 803 kA/m higher than that of S650 °C. According to the demagnetization curves in

Fig. 1(b) and (c), it can be clearly seen that the squareness (Q) of the deformed magnets prepared by HP at different temperatures is much better than that of deformed magnets prepared by SPS at different temperatures.

Figure 2(a) and (b) show the XRD patterns of the hot-deformed magnets prepared by HP and SPS respectively. All the patterns show the presence of the $Nd_2Fe_{14}B$ phase. The peak intensity ratio, $I_{(006)}/I_{(105)}$, is usually used to characterize the degree of texture [28]. It can be observed from Fig. 2(a) that the value of $I_{(006)}/I_{(105)}$ gradually increases by increasing the deformation temperature. As can be seen in Fig. 2(b), the value of $I_{(006)}/I_{(105)}$ is the highest for S650 °C. The increasing value of $I_{(006)}/I_{(105)}$ indicates that the orientation of grains is enhanced and the remanence (J_r) increases. The XRD results are consistent with the magnetic properties.

Figure 3(a) shows the schematic diagram of the HP process. When an alternating current is loaded on the induction coil, an alternating magnetic field is generated. The magnetic flux of the magnetic line passing through the workpiece changes and induced electromotive force inside the workpiece, which then generates an induced current. This current flows inside the workpiece in the circumferential direction of the workpiece, called eddy current. The eddy current generates heat on the workpiece based on the Joule-Lenz law and completes heating. That is, when the sample is prepared by a hot pressing furnace, the heat transfer direction is transferred from the surface of the mold to the sample in the mold cavity (surface of mold is heat source). Figure 3(b) and (c) show the schematic diagram of the SPS. In the SPS, particle discharge, conductive heating, and pressurization are the three main characteristics [29–31]. In addition to the characteristics of both traditional sintering methods, i.e., heating and pressing, the plasma produced by discharge between powder particles has a very high temperature which can generate

**Fig. 2** XRD patterns of hot-deformed magnets: (a) prepared by HP, (b) prepared by SPS

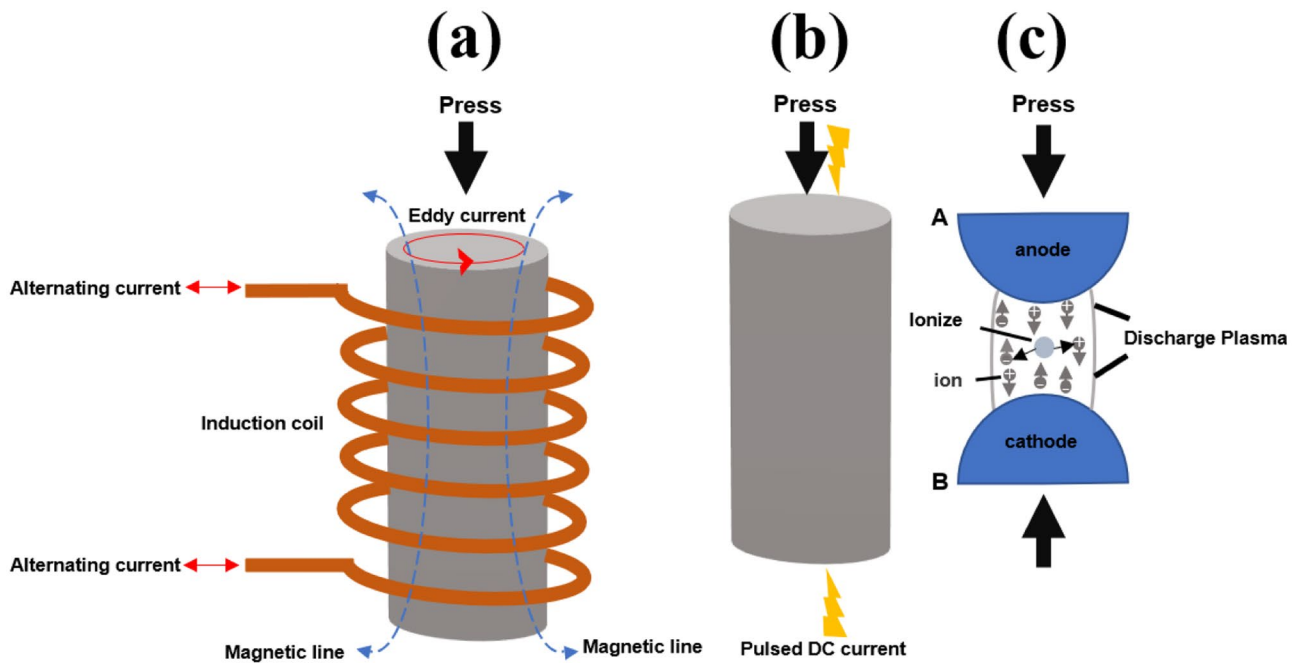


Fig. 3 Schematic diagram of heating principle (a) HP, (b) SPS, particle discharge in SPS (c)

local high temperatures on the surface of the particles. The principle of inter-particle discharge is shown in Fig. 3(c). As the pulse current increases, a pulse voltage is generated between the particles, causing a discharge effect between adjacent particles [32]. When SPS is used to prepare samples, the heat transfer direction is from the sample in the mold cavity to the surface of the mold (sample in the mold cavity is the heat source). This also explains why the deformation temperature of the HP is higher than that of the SPS.

Figure 4(a)–(e) show the low magnification SEM images of the deformed magnets prepared by SPS at different hot deformation temperatures. Figure 4(a) and (b) can clearly distinguish the coarse and fine crystal regions, and the grain size in the fine crystal regions is uniform without any larger crystal grains. When the temperature reaches 700 °C, compared with S600 °C and S650 °C, the average grain size of S700 °C significantly increases, and very large grains appear in the fine grain area as shown in Fig. 4(c). When the temperature continues to rise, the number of abnormally grown grains in the fine-grained region of the S750 °C sample increases, forming a new coarse-crystalline region, while the previous coarse-crystalline region continues to grow. In Fig. 4(e), the coarse and fine crystal regions cannot be distinguished, and the areas of the two crystal regions are the same. Figure 4(f)–(j) are high-magnification images corresponding to the local regions in Fig. 4(a)–(e). As the temperature increases, the width of the coarse grain region of the sample S650 °C is

slightly increased compared to that of S600 °C, as shown in Fig. 4(f) and (g). However, the intrinsic coercivity of the sample S650 °C is higher than that of S600 °C. This may be because the width of the coarse grain zone of the sample at S650 °C increases very little compared with that of S600 °C, and the increase of temperature enhances the fluidity of Nd-rich phase and enables it to distribute among grains more evenly, thus achieving demagnetization coupling between grains [7]. As the temperature rises, the grain orientation of the sample S650 °C is also better than that of S600 °C, as shown in Fig. 4(f) and (g). The grains in the coarse-grain region of Fig. 4(h)–(j) are getting larger and larger, which is consistent with Fig. 4(c)–(e).

Figure 5 shows the SEM images of the deformed magnets prepared by HP at different hot deformation temperatures. The sample H780 °C has holes (Fig. 5(a)), and the crystals have almost no orientation (Fig. 5(f)). When the temperature reaches 800 °C, the number of holes decreases (Fig. 5(b)), and the grains have better orientation (Fig. 5(g)). At 820 °C, the pores of the magnet disappear, and coarse crystal regions begin to appear (Fig. 5(c)), and the orientation of the crystal grains can be clearly seen (Fig. 5(h)). As the temperature continues to rise, the width of the coarse-grain region of the magnet increases (Fig. 5(i)), and the crystal grain orientation becomes more obvious. Growth of coarse crystal zone reduces coercivity of magnets. But the increase of grain orientation enhances the remanence of magnets. This is consistent with the experimental data in Fig. 1(b).

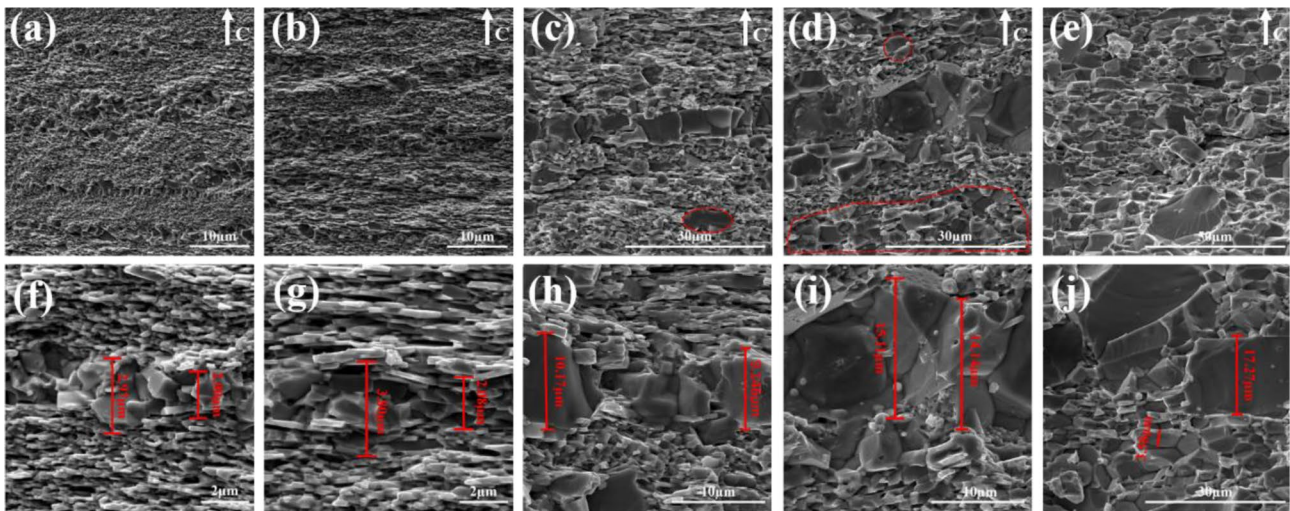


Fig. 4 Low magnification scanning electron microscope (SEM) images of hot-deformed magnets S600 °C (a), S650 °C (b), S700 °C (c), S750 °C (d), and S800 °C (e) prepared by SPS at different temper-

ature. (f) – (j) are high-magnification scanning electron microscope images, corresponding to the coarse crystal region in (a) – (e) respectively

It can be seen from Figs. 4 and 5 that, although the hot deformation temperature of SPS is much lower than that of the HP, the crystal grains of the hot-deformed magnet prepared by SPS are much larger than those prepared by the HP. This is due to the sintering principle and temperature measurement method of the two methods. When SPS is used to prepare samples, the heat source is the sample in the mold cavity, that is, the temperature of the sample in the mold cavity is higher than that of the mold surface. The heat source of HP sample preparation is located

on the surface of the mold, that is, the temperature of the mold surface is higher than that of the sample in the membrane cavity. The temperature measurement of SPS and HP uses thermocouple to measure the temperature of mold surface. This is why the deformation temperature of the hot deformation magnet prepared by SPS is much lower than that of the HP, while the grain growth rate of the hot deformation magnet prepared by SPS is much higher than that of the hot deformation magnet prepared by the HP.

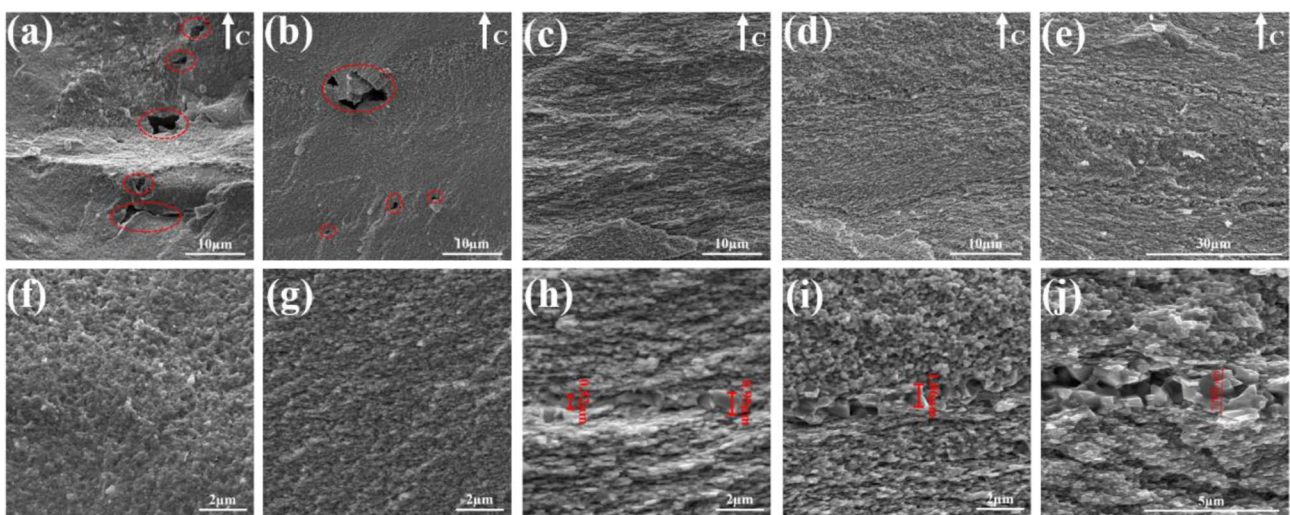


Fig. 5 Low-magnification scanning electron microscope (SEM) images of hot-deformed H780 °C (a), H800 °C (b), H820 °C (c), H840 °C (d), and H860 °C (e) magnets prepared by HP at different temper-

ature. (f) – (j) are high magnification scanning electron microscope images, corresponding to local regions in (a) – (e) respectively

Figure 6(a) and (c) are low-magnification SEM images of sample S650 °C and H860 °C on the c-plane, respectively. Figure 6(a) shows that the sample S650 °C presents large Nd-rich phase aggregation on the c-plane, and the area of Nd-rich phase enrichment is nearly half of the whole picture area. However, in the sample H860 °C, the liquid phase distribution on c-plane is obviously more uniform, as shown in Fig. 6(c). Figure 6(b) and (d) show the high-magnification SEM images of the liquid-phase enrichment region on the c-plane of S650 °C and H860 °C, respectively. It can be seen from Fig. 6(b) that most grains grow abnormally in the liquid phase-enriched area. Compared with the liquid-phase enrichment area of S650 °C, the area of the massive Nd-rich phase is very small in the c-plane of H860 °C, and no obvious abnormal growth of crystal grains is observed in the liquid-phase enrichment area, as shown in Fig. 6(d). Figure 6(b) and (d) were analyzed by SEM-EDS. It can be seen from the element mapping of Nd-L and Fe-K, in

the SEM images, that the black area represents the matrix phase particles, while the white area represents the blocky Nd-rich phase.

Figure 7(a) and (c) are low-magnification SEM images of sample S650 °C and H860 °C on the ab-plane, respectively. The Nd-rich phase in the magnet tends to be enriched at the c-plane grain boundary, while the Nd-rich phase at the ab-plane grain boundary is relatively rare, and even the existence of the grain boundary is not observed [33, 34]. Therefore, compared with c-plane, the volume fraction of Nd-rich phase on ab-plane is less, but enrichment of Nd-rich phase is also observed in various areas on the ab-plane at S650 °C, as shown in Fig. 7(a). Compared with S650 °C, the liquid phase distribution on ab-plane surfaces of H860 °C samples is obviously more uniform, as shown in Fig. 7(c). Figure 7(b) and (d) show the high-magnification SEM images of the liquid-phase enrichment region on the ab-plane of S650 °C and H860 °C, respectively. Figure 7(d) shows that

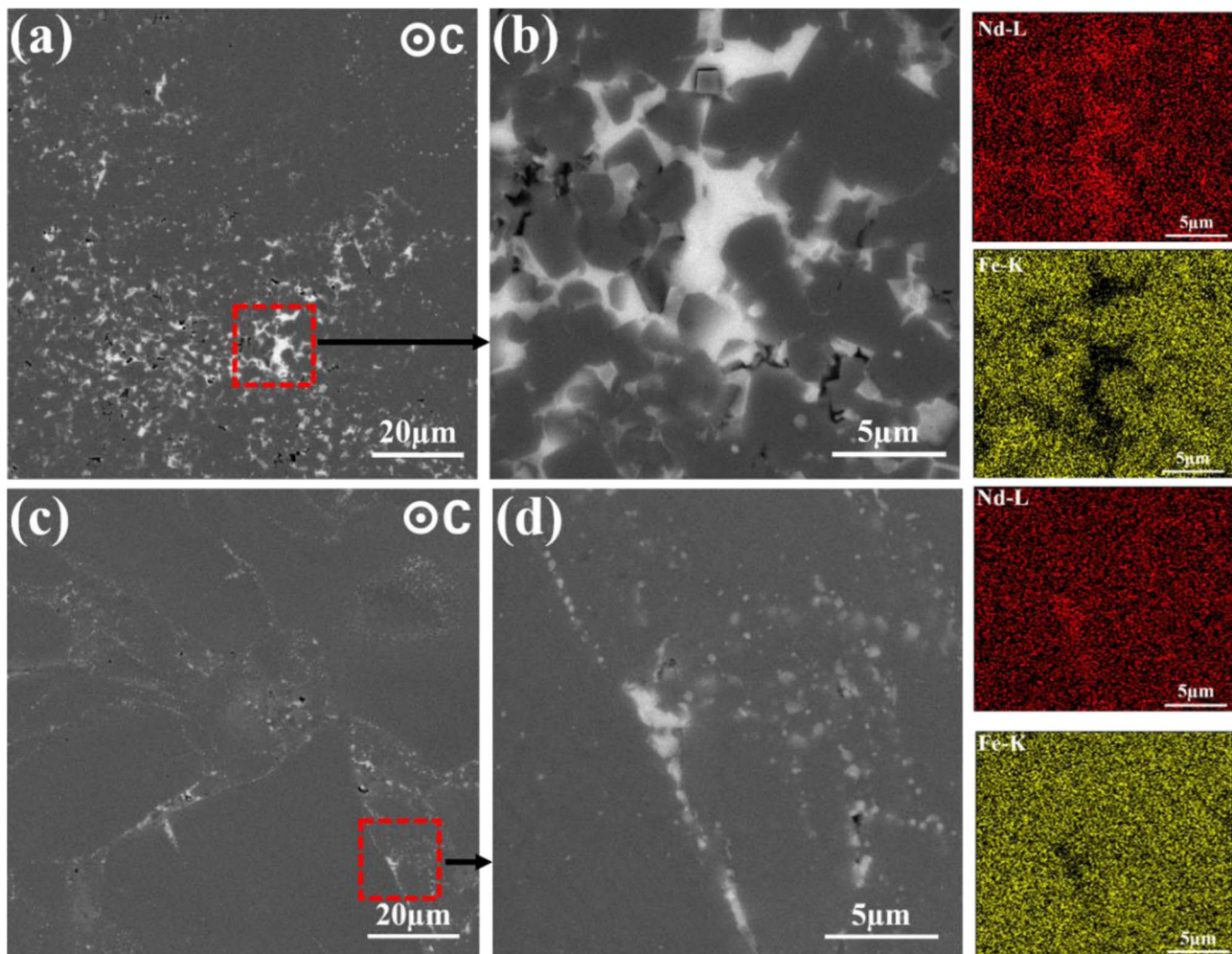


Fig. 6 Low-magnification BSE SEM image of c-plane of (a) S650 °C and (c) H860 °C. BSE SEM images (b) and (d) correspond to the specified areas in images (a) and (c) respectively. SEM-EDS elemental mappings for Nd-L, Fe-K from the same region as (b) and (d)

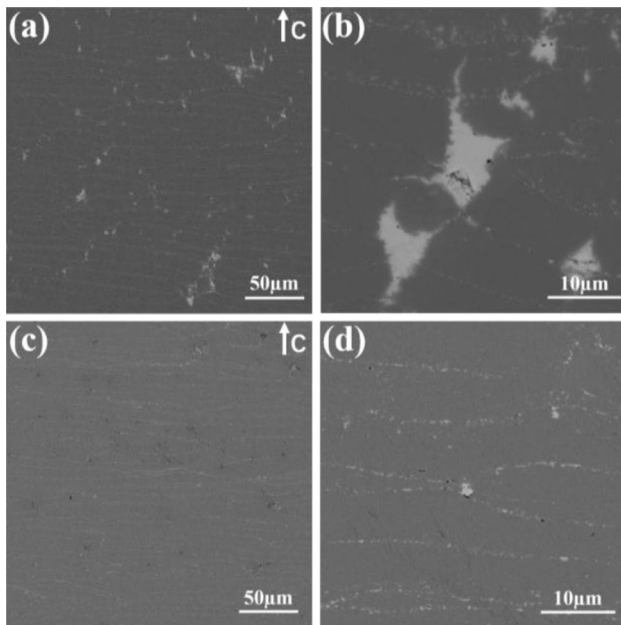


Fig. 7 Low-magnification BSE SEM image on ab-plane of (a) S650 °C and (c) H860 °C; high-magnification BSE SEM image (b) and (d), corresponding to local regions in images (a) and (c) respectively

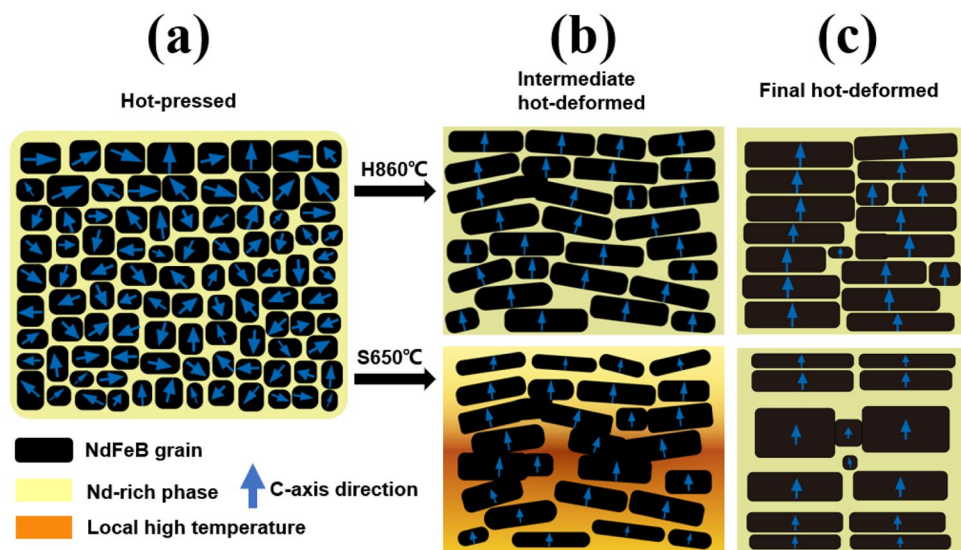
the liquid phase of H860 °C on the ab-plane is uniform and almost has no enrichment. However, S650 °C shows serious liquid phase enrichment on both ab-plane and c-plane, as shown in Figs. 7(b) and 6(b).

By comparing Fig. 6 with Fig. 7, it can be seen that the liquid phase distribution on the surface of S650 °C and H860 °C is significantly different. For S650 °C, severe enrichment of Nd-rich phase and abnormal grain growth near the liquid phase were observed. It is well known that the abnormal growth of crystal grains causes a decrease in the intrinsic coercivity of the magnet [8, 9]. It has been shown that when the Nd-rich phase is severely enriched at the triple junction,

the Nd concentration of the intergranular phase will decrease [9]. Compared with H860 °C, the Nd-rich phase at S650 °C is excessively enriched at the triple junctions. This leads to the reduction of intrinsic coercivity of S650 °C. Due to the extremely uneven liquid phase distribution and the abnormal growth of crystal grains of the magnet prepared by SPS, the squareness of the hot-deformed magnet prepared by SPS is much lower than that of the hot-deformed magnet prepared by the HP [35].

The difference of surface microstructure between S650 °C and H860 °C is due to the different sintering principles of SPS and HP. The mechanism of grain consolidation induced by grain rotation, as an important grain growth mechanism, has been confirmed in many nanocrystalline materials [36–39]. Molecular dynamics simulation and related experiments have proved that the growth rate of grain rotation induced merger during the heat treatment of nanocrystalline materials is much faster than the grain growth mechanism dependent on atomic diffusion [36, 39, 40]. Due to the interparticle discharge in the heating mode of SPS, local high temperature is generated. In the process of the deformation, the liquid phase fluidity in the local high temperature region is enhanced. When the grains are deformed and rotated, it is easy to extrude the grain boundary phase between grains, so that the liquid phase in the high-temperature region is enriched in the triangular grain boundary. There is no grain boundary phase between the grains and they contact each other directly. The grains in contact with each other merge and grow at high temperature [41]. During the hot deformation of the HP, due to its uniform heating without local high temperature, the liquid phase distribution is more uniform when the grain rotates, and there are fewer areas that produce a large amount of liquid phase enrichment, so that its microstructure is more uniform. The grain growth model of S650 °C and H860 °C is shown in Fig. 8.

Fig. 8 Grain growth model of H860 °C and S650 °C



4 Conclusions

In summary, we investigated and compared the effects of the sintering by SPS and HP on the microstructure and magnetic properties of hot-deformed NdFeB magnets. In the hot deformation stage, the temperature of the mold surface is much higher than that of the sample in the cavity in HP, but lower than that of the sample in SPS. Although the hot deformation temperature of SPS is significantly lower than that of HP, the grain growth rate and grain size of the hot-deformed magnets prepared by SPS is far higher than that of the hot-deformed magnets prepared by HP.

Due to inter-particle discharge in the sintering process of SPS, a local high temperature phenomenon occurs, which enhances the liquid phase fluidity. Therefore, the liquid phase between grains is easier to squeeze to the triangular grain boundary and enrich when the grains rotate and merge. Moreover, the high temperature also causes the abnormal growth of grains in this region. However, HP does not enrich large amount of liquid phase like SPS because of its uniform heating.

Compared with HP, the microstructure of hot-deformed magnets prepared by SPS is extremely uneven due to the abnormal growth of grains and the serious enrichment of liquid phase, which is very unfavorable to the magnetic properties.

Funding This work was supported by the National Natural Science Foundation of China (Grant Nos. 51901089 and 52061015), the Key Research and Development Program of Jiangxi Province (No. 20201BBE51010), China Postdoctoral Science Foundation (Grant No. 2020M682064), Postdoctoral Science foundation of Jiangxi Province (Grant No. 2020KY19), the Program of Qingjiang Excellent Young Talents of Jiangxi University of Science and Technology (No. JXUSTQJYX2020003), and the Science and Technology Bureau of Ganzhou City (No. 204301000105).

References

- Lee, R.W., Brewer, E.G., Schaffel, N.A.: *IEEE Trans. Mag.* **21**, 1958–1963 (1985)
- Kirchner, A., Thomas, J., Gutfleisch, O., Hinz, D., Müller, K.-H., Schultz, L.: *J. Alloy. Compd.* **365**, 286–290 (2004)
- Rehman, S.U., Huang, Q.F., Sagar, R.U.R., Jiang, Q.Z., Yang, M.N., Zhong, Z.C.: *J. Magn. Magn. Mater.* **537**, 168237 (2021)
- Li, J., Liu, L.H., Sepehri-Amin, H., Tang, X., Ohkubo, T., Sakuma, N., Shoji, T., Kato, A., Schrefl, T., Hono, K.: *Acta Mater.* **161**, 171–181 (2018)
- Jiang, Q.Z., Song, J., Huang, Q.F., Rehman, S.U., He, L.K., Zeng, Q.W., Zhong, Z.C.: *J. Mater. Sci. Technol.* **58**, 138–144 (2020)
- Jiang, Q.Z., Lei, W.K., He, L.K., Zeng, Q.W., Rehman, S.U., Zhang, L.L., Liu, R.H., Ma, S.C., Zhong, Z.C.: *J. Alloy. Compd.* **775**, 449–456 (2019)
- Liu, J., Sepehri-Amin, H., Ohkubo, T., Hioki, K., Hattori, A., Schrefl, T., Hono, K.: *Acta Mater.* **61**, 5387–5399 (2013)
- Lin, M., Wang, H.J., Yi, P.P., Yan, A.R.: *J. Magn. Magn. Mater.* **322**, 2268–2271 (2010)
- Liu, J., Sepehri-Amin, H., Ohkubo, T., Hioki, K., Hattori, A., Schrefl, T., Hono, K.: *Acta Mater.* **82**, 336–343 (2015)
- Mo, W.J., Zhang, L.T., Shan, A., Cao, L.J., Wu, J.S., Komuro, M.: *Intermetallics* **15**, 1483–1488 (2007)
- Zheng, J., Guo, Z.H., He, Y.N., Li, M.Y., Zhang, M.L., Zhu, M.G., Li, W.: *J. Magn. Magn. Mater.* **488**, 165353 (2019)
- Zheng, J., Guo, Z.H., Li, M.Y., He, Y.N., Wang, X., Zhu, M.G., Li, W.: *J. Alloy. Compd.* **792**, 519–528 (2019)
- Huang, Y.L., Liu, Z.W., Zhong, X.C., Yu, H.Y., Gao, X.X.: *J. Appl. Phys.* **111**, 033913 (2012)
- Lipiec, W., Davies, H.A.: *J. Alloy. Compd.* **491**, 694–697 (2010)
- Jiang, Q.Z., He, L.K., Lei, W.K., Zeng, Q.W., Rehman, S.U., Zhang, L.L., Liu, R.H., Li, J.J., Ma, S.C., Zhong, Z.C.: *J. Magn. Magn. Mater.* **475**, 746–753 (2019)
- He, L., Li, J.J., Yu, X.Q., Rehman, S.U., Qu, P.P., Li, F.F., Hu, Y.T., Huang, Q.F.: *IEEE Trans. Magn.* **57**, 1–7 (2021)
- Song, J., Jiang, Q.Z., Rehman, S.U., He, L.K., Li, X., Chen, Y.W., Zhao, C.J., Zhong, Z.C.: *Physical B.* **605**, 412711 (2021)
- Hou, Y.H., Huang, Y.L., Liu, Z.W., Zeng, D.C., Ma, S.C., Zhong, Z.C.: *Mater. Sci. Eng. B* **178**, 990–997 (2013)
- Wuest, H., Bommer, L., Weissgaerber, T., Kieback, B.: *J. Magn. Magn. Mater.* **392**, 74–78 (2015)
- Li, Y.Q., Xu, X.C., Yue, M., Ma, T.Y., Liu, W.Q.: *J. Magn. Magn. Mater.* **508**, 166847 (2020)
- Korenta, M., Komelj, M., Šturm, S., Rožman, K. Ž., Kobe, S., Soderžnik, K. Ž., Soderžnik, M.: *J. Magn. Magn. Mater.* **515**, 167279 (2020)
- Castle, E., Sheridan, R., Grasso, S., Walton, A., Reece, M.: *J. Magn. Magn. Mater.* **417**, 279–283 (2016)
- Ulrich, S.R., Frank, K., Rainer, G.: *J. Eur. Ceram. Soc.* **38**, 3585–3594 (2018)
- Lee, M.H., Park, J.H., Park, S.D., Rhyee, J.S., Oh, M.W.: *J. Alloy. Compd.* **786**, 515–522 (2019)
- Zhang, X.R., Zhang, Z.X., Wen, R.L., Wang, G.S., Zhang, X.L.: *Ceram. Int.* **44**, 2615–2619 (2018)
- Chen, F.G., Zhang, T.Q., Wang, J., Zhang, L.T., Zhou, G.F.: *Scr. Mater.* **107**, 38–41 (2015)
- Chen, B., Li, J., Liu, Y., Wang, R.Q., Lian, L.X.: *Rare Met.* **33**, 448–451 (2014)
- Huang, X.Y., Li, J.J., Rehman, S.U., Qu, P.P., He, L., Zeng, L.L., Yu, X.Q., Yang, M.N., Zhong, Z.C.: *J. Magn. Magn. Mater.* **503**, 166637 (2020)
- Chen, W., Anselmi-Tamburini, U., Garay, J.E., Groza, J.R., Munir, Z.A.: *Mater. Sci. Eng. A.* **394**, 132–138 (2005)
- Anselmi-Tamburini, U., Gennari, S., Garay, J.E., Munir, Z.A.: *Mater. Sci. Eng. A.* **394**, 139–148 (2005)
- Anselmi-Tamburini, U., Garay, J.E., Munir, Z.A.: *Mater. Sci. Eng. A.* **407**, 24–30 (2005)
- Omori, M.: *Mater. Sci. Eng. A.* **287**, 183–188 (2000)
- Sepehri-Amin, H., Ohkubo, T., Nagashima, S., Yano, M., Shoji, T., Kato, A., Schrefl, T., Hono, K.: *Acta Mater.* **61**, 6622–6634 (2013)
- Liu, J., Sepehri-Amin, H., Ohkubo, T.: *J. Appl. Phys.* **115**, 17A774 (2014)
- Pérido, E. A., Takiishi, H., Motta, C. C., Faria, R. N.: *J. Appl. Phys.* **102**, 113912 (2007)
- Hu, J., Shen, Z.: *Acta Mater.* **60**, 6405–6412 (2012)
- Chaim, R.: *Scr. Mater.* **66**, 269–271 (2012)
- Lee, C.H., Lu, H.H., Wang, C.A.: *J. Am. Ceram. Soc.* **94**, 1182–1190 (2011)
- Haslam, A., Phillpot, S., Wolf, D., Moldovan, D., Gleiter, H.: *Mater. Sci. Eng. A.* **318**, 293–312 (2001)

40. Wang, L., Hu, J., Cheng, Y., Fu, Z., Shen, Z., Xiong, Y.: *Scr. Mater.* **107**, 59–62 (2015)
41. Fang, Z.Z., Wang, H.: *Int. Mater. Rev.* **53**, 326–352 (2008)

Publisher's Note Springer Nature remains neutral with regard to jurisdictional claims in published maps and institutional affiliations.